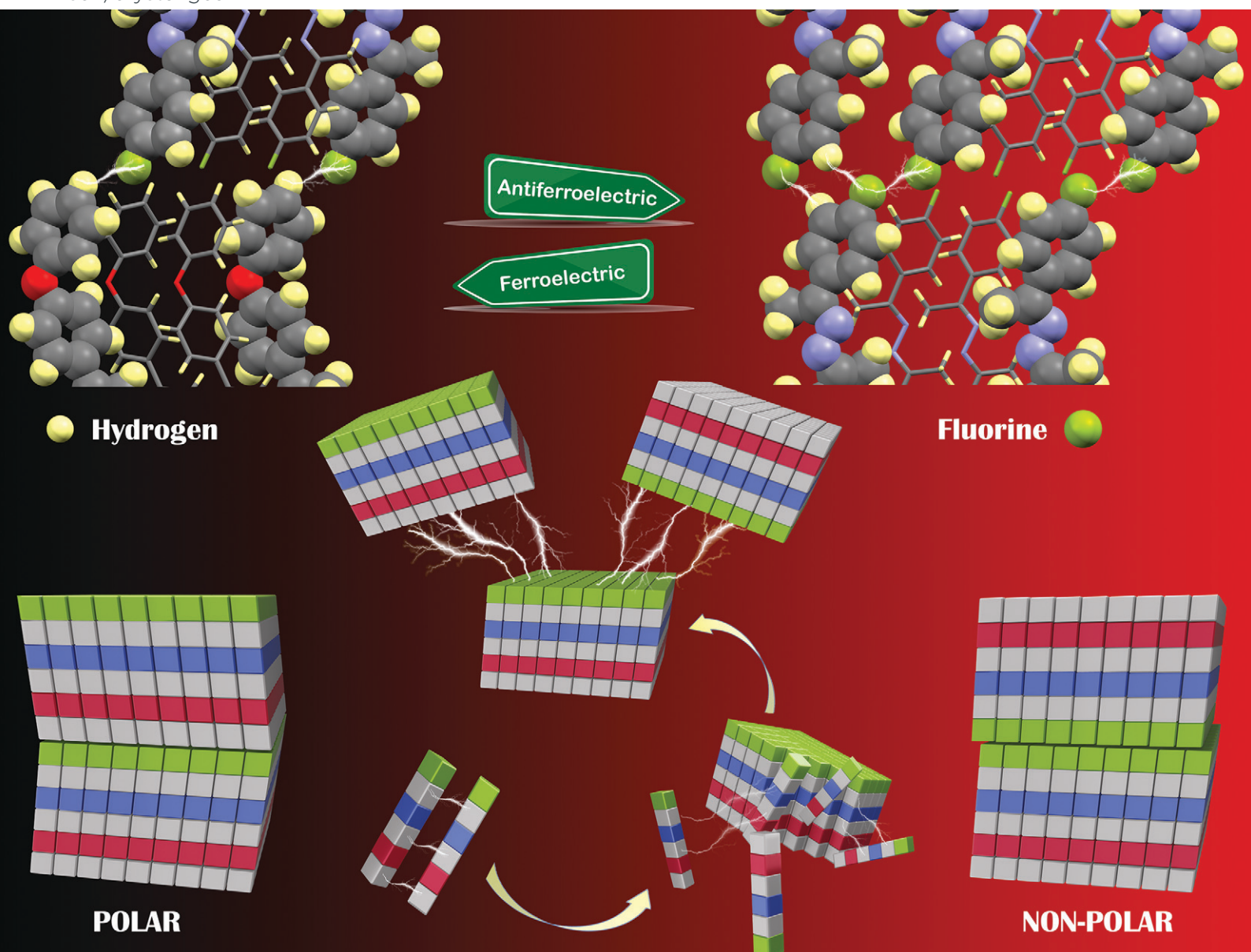


CrystEngComm

rsc.li/crystengcomm



ISSN 1466-8033

COMMUNICATION

Rainer Glaser *et al.*

Polar and non-polar stacking of perfectly aligned parallel
beloamphiphile monolayers (PBAMs) of (PhO, F)-azine.
The interplay of non-covalent interlayer interactions and
unit cell polarity


 Cite this: *CrystEngComm*, 2023, 25, 2175

 Received 6th January 2023,
Accepted 16th March 2023

DOI: 10.1039/d3ce00021d

rsc.li/crystengcomm

Polar and non-polar stacking of perfectly aligned parallel beloamphiphile monolayers (PBAMs) of (PhO, F)-azine. The interplay of non-covalent interlayer interactions and unit cell polarity†

 Harmeet Bhoday, ^a Steven P. Kelley ^b and Rainer Glaser ^{*a}

Polar and non-polar polymorphs of (PhO, F)-azine are reported. Both polymorphs feature identical 2-D perfectly parallel-aligned beloamphiphile monolayers (PBAMs). The striking contrast between the polymorphs is the stacking of the PBAMs in the third dimension. The difference in stacking demonstrates the subtle role of weak non-covalent interlayer interactions and unit cell polarity in affecting the crystal architecture.

Polar donor–acceptor substituted organic molecular crystals are promising for their wide range of applications in the realm of non-linear optics (NLO), terahertz generation, electro-optics, ferroelectricity, photovoltaics, and fluorescence.^{1–8} However, the achievement of dipole parallel alignment in organic donor–acceptor substituted molecular crystals has been challenging as there are only very few molecules that result in any ferroelectric crystals. The key issue in producing a polar crystal arises from the fact that side-by-side polar molecules avoid parallel alignment due to electrostatic reasons and only the collinear molecules prefer parallel alignment. In general, most polar molecules would crystallize in a way as to compensate for the dipole moments producing a non-polar crystal. It was believed for a long time that achieving any polar order is almost impossible as the electrostatic repulsions related to parallel alignment are invincible. However, our calculations have shown that parallel aligned dipole lattices may occur as local minima.⁹ Hence, the rational design of polar molecular crystals is feasible.

Our rational design approach consists of two steps: dipole-moment minimization and taking advantage of intralayer

intermolecular interactions. If the donor and acceptor are chosen such that the molecule has a moderate dipole moment the electrostatic repulsion can be reduced. Second, we make use of intralayer arene–arene interactions to further assist the stabilization of parallel alignment. Following our rational design strategy, we have been able to grow polar crystals for a variety of donor(X)–acceptor(Y) acetophenone azines (C=N–N=C spacer group), which we refer to as (X,Y)-azines. Specifically, perfect polar order throughout the PBAMs has been achieved first with the X = methoxy series (Y = Cl, Br, I)^{10–12} and recently with the X = phenoxy series (Y = F, Cl, Br, I).^{13,14} Both series feature polar stacking of the 2-D layers in the third dimension and perfect polar stacking was achieved for (PhO, Y)-azines with Y = Cl, Br, I.

The case of (PhO, F)-azine is a special one as we were able to grow two polymorphs, **I** and **II**. Much to our initial surprise, in **I** the PBAMs stack in an antiparallel fashion to give rise to a non-polar crystal.¹⁵ Only later did we obtain polymorph **II** which realizes the electrostatically expected polar PBAM stacking. In contrast to the perfect polar alignment achieved with the other halogens, polymorph **II** of (PhO, F)-azine features near-perfect dipole alignment because of the zigzag arrangement of its PBAMs (*vide infra*). Polymorph **I** crystallizes in triclinic space group $P\bar{1}$ while **II** in orthorhombic space group $Pna2_1$. The reflections for polymorph **I** were recorded at 100 K (**Ia**) and 293 K (**Ib**)¹⁵ while the reflections for polymorph **II** were recorded at 100 K (**IIa**)¹⁶ and 150 K (**IIb**).¹⁴ Crystal structure details of these forms are listed in Table S1 (ESI†) and we only discuss the low temperature forms **Ia** and **IIa**, which we will refer to as **I** and **II**.

Azine molecules are characterized by the torsion angle $\tau = \angle(\text{C}=\text{N}-\text{N}=\text{C})$ and the phenyl twist dihedral angles $\varphi = \angle(\text{C}-\text{C}-\text{C}=\text{N})$ on both sides; with φ_{PhO} on the phenoxy side and φ_{F} on the fluorine side as shown in Fig. 1.

There are two symmetry independent molecules **A** and **B** for polymorph **I** while polymorph **II** contains only one unique molecule **A**. The unique molecules are a side-by-side pair in

^a Department of Chemistry, Missouri University of Science and Technology, 302 Schrenk Hall, 400 W. 11th St., Rolla, MO 65409, USA. E-mail: glaserr@mst.edu

^b Center for Crystallography, University of Missouri, 26 Schlundt Hall, Columbia, MO 65211, USA

† Electronic supplementary information (ESI) available: Experimental details and results of GC/MS, ¹H-, ¹⁹F-, ¹³C-NMR, and solid-state FTIR analyses, additional tables, figures, Hirshfeld fingerprint plots and lattice energies. CCDC 2013773, 2013774, 2103130 and 2234129. For ESI and crystallographic data in CIF or other electronic format see DOI: <https://doi.org/10.1039/d3ce00021d>



Fig. 1 Chemical structure and ORTEP diagram of (PhO, F)-azine.

the unit cell with opposite helicity. In molecules with *P*-helicity the proximate N=C bond is rotated clockwise to eclipse the distal C=N bond. Each unit cell contains four molecules with two side-by-side pairs in adjacent PBAMs, see Fig. S7 and S8 (ESI[†]). Table 1 lists the values for τ , φ_{PhO} and φ_{F} for the three unique azine molecules. It is noteworthy that these dihedral angles differ only slightly because of the great similarity of the intralayer intermolecular interactions in **I** and **II**. Complete lists of bond lengths, bond angles, and other torsion angles for **I** and **II** are provided in Table S3–S5 (ESI[†]).

Perfect polar alignment is realized in the 2D monolayers for both the polymorphs **I** and **II**. Fig. 2 shows the schematic representation of the (PhO, F)-azine PBAMs. The molecules in the PBAM are held together by various intralayer intermolecular interactions and one pair is shown in Fig. 2. The most important intralayer interactions are C–H \cdots π interactions.^{17,18} An arene–arene T-contact occurs when a C–H bond acts as an edge (e) pointing toward the center of an arene face (f). Every pair of azines interacts *via* three T-contacts and the molecular model shown on the right in Fig. 2 exemplifies the (f|e|f|e) triple T-contact in the PBAMs.

The PBAMs in **I** and **II** are very similar and their overlay in Fig. S10 (ESI[†]) clearly shows almost perfect overlap in the azine regions with tiny differences at the phenoxy and fluoro ends of the molecules. We argue that these differences arise from interlayer interactions rather than the intralayer interactions. This assertion is well supported by the Hirshfeld fingerprint plots^{19–21} (Fig. S13, ESI[†]) for the symmetry independent molecules **I-A**, **I-B** and **II-A** and the percent contributions to their 2D plots. The values representing the relevant intralayer interactions are barely different and shown in black, while noticeable differences occur between

Table 1 Torsion angles in **I** and **II**

\angle	Form I		Form II
	A ^a (<i>P</i>)	B ^a (<i>M</i>)	A ^a (<i>P</i>)
τ	143.76°	–143.76°	143.84°
φ_{PhO}	179.85°	–179.69°	179.83°
φ_{F}	178.64°	–179.23°	179.19°

^a **A** and **B** refer to the two unique molecules in **I**.

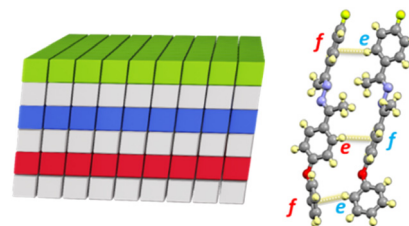


Fig. 2 Schematic representation of a parallel belowamphiphile monolayer (PBAM) in the crystal structures **I** and **II** of (PhO, F)-azine; green: fluorine, grey: arene, blue: azine, red: phenoxy. The pair shown on the right exemplifies the (f|e|f|e) triple T-contact in the PBAMs where one azine interacts with two faces and one edge (f|e|f) and the other with one face and two edges (e|f|e).

the values for interlayer interactions, which are emphasized in red.

To avoid redundancy, we elaborate on intralayer interactions in PBAMs of polymorph **I**. Fig. 3(a) shows the fragment of the PBAM in **I** to illustrate the environment of a starred molecule A*. The term “stripe” refers to a column of molecules of one type and **I** contains stripes composed of unique molecules **A** or **B**. The molecule A* is surrounded by six neighbors in three stripes and engages in five unique pair

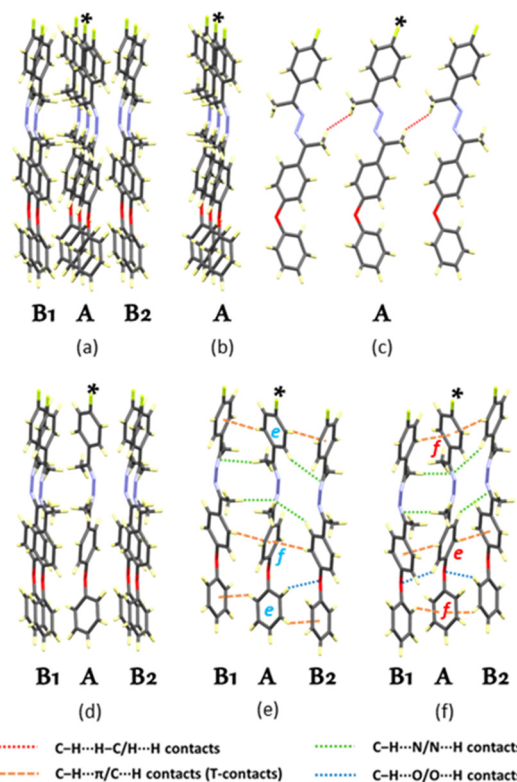


Fig. 3 Intralayer interactions. (a) A fragment of the PBAM in **I** shows the starred A* molecule surrounded by six neighbours in the A stripe and the two neighbouring B stripes. Interactions within the A stripe shown in (b) and (c) from different viewpoints. Interactions of the starred molecule with molecules in the B stripes are shown in (d). The starred molecule functions as (e|f|e) synthon as shown in (e) and as (f|e|f) synthon in (f).

interactions. Interactions within the **A** stripe are illustrated in Fig. 3(b) and (c); there is no π -stacking in the **A** stripes and pairs of **A** molecules benefit only from weak C–H \cdots H–C contacts shown as red dotted lines in Fig. 3(c). Interactions of **A*** with four molecules in stripes **B**₁ and **B**₂ are shown in Fig. 3(d). All molecules in stripes **B**₁ and **B**₂ are identical and of opposite helicity compared to the molecules in stripe **A**. **A*** engages as (e|f|e) synthon in two pair interactions shown in Fig. 3(e) and as (f|e|f) synthon in two more pair interactions shown in Fig. 3(f) to form four triple T-contacts, two of the (ef|fe|ef) type and two of the (fe|ef|fe) type. Note that the two (ef|fe|ef) contacts with the **B**₁ and **B**₂ molecules are topologically different and the same is true for the two (fe|ef|fe) contacts.

While the nomenclature of the (ef|fe|ef) and (fe|ef|fe) contacts emphasizes arene-arene interactions (C–H \cdots π , orange), the pair interactions also benefit from weak C–H \cdots N contacts (green) and C–H \cdots O contacts (blue). C–H \cdots N contacts are produced when a phenyl or methyl C–H interacts with one azine-N in the adjacent stripe and **A*** forms eight such contacts and acts as the N-part in four of them. **A*** engages its N_{PhO} in the two contacts of Fig. 3(e) while it engages its N_F in the two contacts of Fig. 3(f). Regarding the C–H \cdots O contacts, two ortho C–H bonds of the diphenyl ether moiety may engage either from the Ph_{PhO} and Ph_{end} arenes. **A*** functions as the O-part in one (**B**₂)C–H \cdots O contact, as C–H(Ph_{PhO}) in one C–H \cdots O(**B**₁) contact, and as C–H(Ph_{end}) in one C–H \cdots O(**B**₂) contact.

The Hirshfeld fingerprint plots for **I-A** in Fig. 4 allow to distinguish all these *intralayer* interactions and inform about their relative significance. The triple T-contacts are the crucial intralayer interactions as is evident from the spiked and most intense fingerprint plot for the C \cdots H contacts. The strengths of these interactions were quantified using the aromatic analyser tool in CSD-Mercury and the scores of 8.7–9.0 represent highly favorable aromatic interactions (Table

S6, ESI†). This result provides compelling evidence that triple T-contacts are significantly stabilizing and structure-directing. Although, C–H \cdots H–C contacts are associated with more than 40% of the surface area of the fingerprint plot, only the one close H \cdots H contact of Fig. 3(c) corresponds to the spike in the middle of the fingerprint plot. The other H \cdots H contacts only contribute slightly to PBAM stability. Additional contribution to PBAM stability is attributed to C–H \cdots O contacts and a pair of spikes manifest these interactions and their directional nature. There are no pronounced spikes in the plot of C–H \cdots N contacts. Lastly, C \cdots C and C \cdots N/C \cdots O contacts essentially do not contribute to PBAM stability.

We calculated pairwise interaction energies for molecules within 3.8 Å of the reference molecule **A*** in **I-A** (Fig. S17, ESI†) at the B3LYP/6-31G(d,p) level^{22,23} as embedded in *CrystalExplorer* (Table S8, ESI†). The intralayer interactions between **A*** and four molecules in the **B** stripe are most binding with total energies of –54.5, –55.0, –59.0, and –59.2 kJ mol^{–1}. This stabilization can be attributed to triple T-contacts, C–H \cdots O contacts, and C–H \cdots N contacts. The C–H \cdots H–C interaction of **A*** with its neighbors in the **A** stripe is modest with an energy of –21.4 kJ mol^{–1}. Similar calculations were performed for **I-B** and **II** (Fig. S18 and S19, Tables S9 and S10, ESI†). These pairwise interaction energies provide strong support of the structural discussion and the Hirshfeld analysis of intralayer binding.

The central question of the present paper concerns the origin of the difference in the PBAM stacking of polymorphs **I** and **II**. With the above discussion of the PBAMs we are now in a position to address this crucial question. For electrostatic reasons, it would be expected that the PBAMs stack in a polar fashion. This expectation is met in the observed dipole parallel stacking in **II** but unexpectedly the

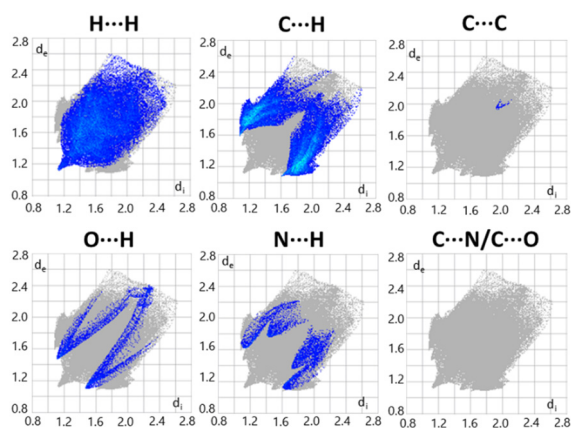


Fig. 4 Hirshfeld fingerprint plots for molecule **I-A** resolved into H \cdots H, C \cdots H, C \cdots C, O \cdots H, N \cdots H, C \cdots N/C \cdots O contacts. The analogous plots for **I-B** and **II-A** are essentially the same and are included in the supporting information (Fig. S15, ESI†).

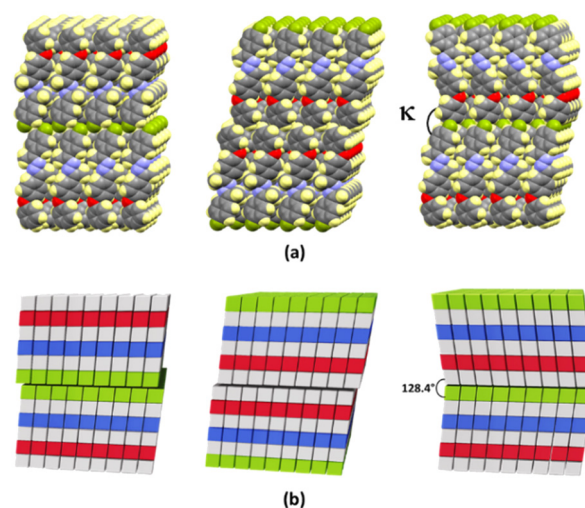


Fig. 5 Bilayer architecture of (PhO, F)-azine: polymorphs **I** (left with F/F interface, center with PhO/PhO interface) and **II** (right with F/PhO interface). (a) Space-filling presentations of their crystal structures and (b) schematic representations to emphasize the dipole antiparallel and parallel alignments, respectively.

PBAMs stack in an antiparallel fashion in **I** (Fig. 5). A more subtle difference concerns the relative orientation of PBAMs along the stacking direction. We define κ as the angle enclosed between the N–N bonds of azines in successive PBAMs. Polymorph **I** features $\kappa = 180^\circ$, whereas the polar stacking in **II** results in a “zigzag pattern” of the PBAMs with $\kappa = 128.4^\circ$. We will now show how non-covalent interlayer interactions between the PBAM surfaces affect their stacking. Three types of surface contacts occur: F/PhO interfaces in **II** and F/F and PhO/PhO interfaces alternate in **I** and interface inter-actions are described in Fig. 6.

There is only one kind of stripe **A** in polymorph **II** and one type of short intermolecular C–H \cdots F contact (2.58 Å). At the F/PhO interface arene–arene parallel displaced π -stacking interactions occur (5.85 Å). The lattice architecture of polymorph **I** is more complicated because each PBAM features two stripes **A** and **B** and because each PBAM engages in F/F and PhO/PhO interfaces. The prominent short contacts in the F/F interface are C–F \cdots F–C contacts (2.89 Å), double C–H \cdots F contacts (2.53 Å), and C–F \cdots F–C contacts (2.80 Å). Only the molecule **B** in **I** features a parallel displaced π -stacking interaction and there are two of them involving the Ph_{end} (5.55 Å) and Ph_F (6.25 Å).

The major contributions to the binding between layers comes from H \cdots F and F \cdots F contacts. The Hirshfeld fingerprint plots in Fig. 7 show that the H \cdots F contacts in **II-A** are condensed into a smaller area. This is in sharp contrast to weak H \cdots Y contacts in the other (PhO, Y)-azines and the case for Y = Cl is made in Fig. S14 and S15 (ESI †). In **I** only the **B** molecules participate in such contacts while the **A**

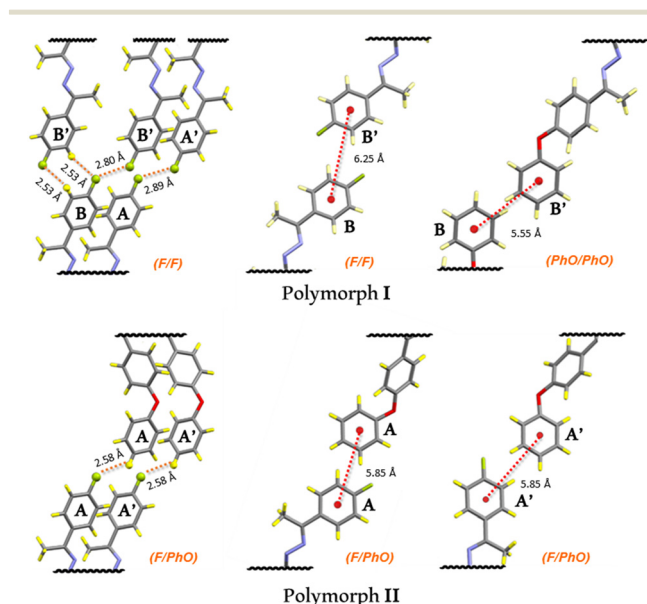


Fig. 6 Interlayer interactions in polymorphs **I** and **II** of (PhO, F)-azine. **I** features alternating stripes **A** and **B**. On the F/F interface molecules in stripe **A** feature C–F \cdots F–C contacts while those in stripe **B** feature both C–H \cdots F and C–F \cdots F–C contacts. On the F/F and PhO/PhO interfaces **I** features parallel displaced arene–arene π -stacking interactions. On the F/PhO interface **II** features C–H \cdots F (left) and parallel displaced arene–arene π -stacking interactions (right).

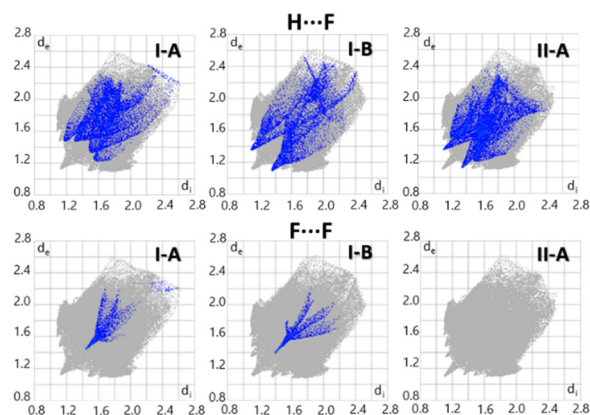


Fig. 7 Hirshfeld fingerprint plots for molecules **I-A**, **I-B**, and **II-A** in polymorphs **I** and **II** resolved into C–H \cdots F (top) and C–F \cdots F–C (bottom) contacts.

molecules do not. These contacts for **I-B** and **II-A** show up as pointed spikes reflecting their directional nature. No such spikes manifest for molecules **I-A**. Both **A** and **B** in **I** form short directional F \cdots F contacts which show up as spikes in the F \cdots F fingerprint plots. In polar stacked **II** there are of course no interlayer F \cdots F contacts and the absence of any features in the bottom right fingerprint plot of **II-A** also shows that there are no lateral F \cdots F contacts within the PBAM surface.

The Tables S8–S10 and Fig. S17–S19 † reporting on pairwise interaction energies include intralayer and interlayer interactions. The former were discussed above and here we discuss the interlayer interactions involving fluorine bonding. The C–H \cdots F interactions in **I** and **II** are of comparable strength and F \cdots F binding is less important. The double C–H \cdots F contact in **I-B** is binding by -11.9 kJ mol $^{-1}$ and the single C–H \cdots F interaction in **II-A** contributes -9.1 kJ mol $^{-1}$ to binding. The molecules engaged in F \cdots F contacts feature pairwise binding energies of -2.2 kJ mol $^{-1}$ in **I-B** and of -4.4 kJ mol $^{-1}$ in **I-A**.

Arene–arene π -stacking interactions contribute only modestly to interlayer binding in both polymorphs. The scores for the strengths of these interactions were calculated using the aromatic analyzer tool in CSD-Mercury (Tables S6 and S7, ESI †) and they fall in the range 5–7 and indicate that their moderate strengths are less likely to lead to optimization of the final crystal stacking architecture.

We computed lattice energies E_{lat} based on the pair interaction energies of molecular electron densities computed at the B3LYP/6-31G(d,p) level^{22,23} as embedded in *CrystalExplorer*, and we also computed lattice energies with the UNI atom-atom intermolecular potentials²⁴ embedded in the CSD-Mercury software (ESI †). The lattice energies E_{lat} determined with these methods are listed in Table 2. The data show that the polymorph preference energies PPE are very small with a slight advantage for polymorph **I**, PPE(CE-B3LYP) = 2.05 kJ mol $^{-1}$ and PPE(UNI) = 0.50 kJ mol $^{-1}$. We have argued that the PBAM architectures in **I** and **II** are

Table 2 Lattice energies of polymorphs I and II

Form	Energy	CE-B3LYP	UNI
I	$E_{\text{lat}}(\text{I-A})$	-171.10	—
	$E_{\text{lat}}(\text{I-B})$	-171.20	—
	$E_{\text{lat}}(\text{I})^{a,b}$	-171.15	-173.00
II	$E_{\text{lat}}(\text{II})$	-169.10	-172.50
	E_{cd}	-4.60	—
	${}^{\text{fe}}E_{\text{lat}}(\text{II})^a$	-173.70	-172.50
II vs. I	PPE ^c	2.05	0.50
	${}^{\text{fe}}\text{PPE}^c$	-2.55	—

^a $E_{\text{lat}} = 0.5 E_{\text{tot}}$; ${}^{\text{fe}}E_{\text{lat}} = E_{\text{lat}} + E_{\text{cd}}$; E_{cd} is the cell dipole energy. ^b $E_{\text{lat}}(\text{I})$ averaged over lattice energies computed for **A** and **B**. ^c PPE = polymorph preference energy; $\text{PPE} = E_{\text{lat}}(\text{II}) - E_{\text{lat}}(\text{I})$; ${}^{\text{fe}}\text{PPE} = {}^{\text{fe}}E_{\text{lat}}(\text{II}) - E_{\text{lat}}(\text{I})$.

structurally and electronically very similar and these findings suggest that the PBAM stabilities also should be very similar in both polymorphs. In other words, a positive PPE value provides strong evidence that the realization of two types of non-covalent interlayer interactions of the non-polar polymorph **I** are preferred over the presence of two equal non-covalent interlayer interactions of polar polymorph **II**. However, we obtained crystals of the non-polar polymorph **I** only once whereas all subsequent crystallization experiments afforded the polar polymorph **II**. Clearly, there is a strong preference for the formation of polymorph **II** and it is related to the electrostatic stabilization between polar unit cells. Polymorph **II** crystallizes in the polar space group $Pna2_1$ and for such ferroelectric crystals the lattice energy ${}^{\text{fe}}E_{\text{lat}}$ requires the cell dipole energy E_{cd} correction as an additional term.²⁵ The value $E_{\text{cd}}(\text{CE-B3LYP}) = -4.60 \text{ kJ mol}^{-1}$ exceeds the respective E_{lat} value in magnitude and leads to a reversal in sign of ${}^{\text{fe}}\text{PPE}$ compared to PPE. With the consideration of the Coulomb stabilization of the polar crystals of polymorph **II**, the ferroelectric lattice energy ${}^{\text{fe}}\text{PPE}(\text{CE-B3LYP}) = -2.55 \text{ kJ mol}^{-1}$ becomes negative and consistent with the outcome of the crystallization experiments.

We previously pointed out that PBAMs can only be formed if the dipole–dipole repulsion between side-by-side azines is moderate and this condition requires an upper limit for the molecular dipole μ_{ul} . The present discussion shows that there also exists a lower limit for the molecular dipole moment μ_{ll} to guarantee polar stacking and a negative value of ${}^{\text{fe}}\text{PPE} = \text{PPE} + E_{\text{cd}}$. Polar stacking will be realized if the E_{cd} and PPE terms have the same negative sign (Scenario 1), it may be realized if the E_{cd} term overcompensates a positive PPE term (Scenario 2), and it will not be realized if E_{cd} cannot compensate a positive PPE term (Scenario 3).

The dipole moment of (PhO, F)-azine¹⁴ is at least 20% smaller than for (PhO, Y)-azines¹⁴ with $Y = \text{Cl, Br, I}$ and therefore the E_{cd} term of (PhO, F)-azine will be the least negative in the series ($E_{\text{cd}} \propto p_{\text{cell}}^2$) and makes the (PhO, F)-azine the most likely azine to realize both stacking options. The data in Table 2 show that both stacking options are

realized for (PhO, F)-azine because the small negative E_{cd} value together with the positive PPE value results in a ${}^{\text{fe}}\text{PPE}$ value of modest magnitude (Scenario 2).

It has been well precedented in previous studies that weak non-covalent intermolecular interactions involving fluorine (C–H \cdots F and C–F \cdots F–C contacts) can play a structural role in crystal packing.^{26–30} In fact, the special bonding features associated with fluorine have enabled the realization of both ferroelectric and antiferroelectric PBAM stacking in (PhO, F)-azine because the antiparallel stacking offers a small but significant advantage for the interlayer binding of the PBAMs.

Author contributions

H. Bhoday: synthesis and crystallization, formal analysis, computational analysis, methodology, visualization, writing; S. P. Kelley: X-ray crystallography, X-ray data curation; R. Glaser: conceptualization, formal analysis, funding acquisition, project administration, resources, supervision and mentoring, writing.

Conflicts of interest

The authors declare no conflict of interest.

Acknowledgements

This work was supported by the Missouri University of Science and Technology.

References

- R. Akiyoshia and S. Hayami, *Chem. Commun.*, 2022, **58**, 8309–8321.
- X. Liu, Z. Yang, D. Wang and H. Cao, *Crystals*, 2016, **6**(12), 158.
- T. Tong, W. Zhang, Z. Yang and S. Pan, *Angew. Chem., Int. Ed.*, 2020, **60**, 1332–1338.
- S. J. Kim, B. J. Kang, U. Puc, W. T. Kim, M. Jazbinsek, F. Rotermund and O. P. Kwon, *Adv. Opt. Mater.*, 2021, **9**, 2101019.
- T. Ghosh, M. Mondal and R. K. Vijayaraghavan, *Mater. Chem. Front.*, 2022, **6**, 297–305.
- L. Mencaroni, C. Bonaccorso, V. Botti, B. Carlotti, G. Consiglio, F. Elisei, C. G. Fortuna, A. Spalletti and A. Cesaretti, *Dyes Pigm.*, 2021, **194**, 109620.
- R. Glaser, *Acc. Chem. Res.*, 2007, **40**, 9–13.
- S. Horiuchi and Y. Tokura, *Nat. Mater.*, 2008, **7**, 357–366.
- D. Steiger, C. Ahlbrandt and R. Glaser, *J. Phys. Chem. B*, 1998, **102**, 4257–4260.
- G. S. Chen, J. K. Wilbur, C. L. Barnes and R. Glaser, *J. Chem. Soc., Perkin Trans. 2*, 1995, 2311–2317.
- M. Lewis, C. Barnes and R. Glaser, *Acta Crystallogr., Sect. C: Cryst. Struct. Commun.*, 2000, **56**, 393–396.
- M. Lewis, C. Barnes and R. Glaser, *J. Chem. Crystallogr.*, 2000, **30**, 489–496.

- 13 CCDC codes for supplementary crystallographic data for parallel-aligned (PhO, Y)-azines with Y = Cl: M. Lewis, H. Bhoday, C. L. Barnes, S. P. Kelley, A. Choudhury and R. Glaser, *CCDC Comm.*, 2020, 2017223 (NUVPUS), Y = Br: M. Lewis, H. Bhoday, C. L. Barnes, S. P. Kelley, A. Choudhury and R. Glaser, *CCDC Comm.*, 2020, 2014691 (KUSNEU, 100 K), 2014692 (KUSNIY, 298 K), Y = I: M. Lewis, H. Bhoday, C. L. Barnes, S. P. Kelley, A. Choudhury and R. Glaser, *CCDC Comm.*, 2020, 2017222 (NUVPOM, 173 K), 2017221 (NUVPIG, 298 K), and Y = F: M. Lewis, H. Bhoday, C. L. Barnes, S. P. Kelley, A. Choudhury and R. Glaser, *CCDC Comm.*, 2020, 2103130 (OBELIU, IIb, 150 K).
- 14 H. Bhoday, M. Lewis, S. P. Kelley and R. Glaser, *ChemPlusChem*, 2022, **87**, e202200224.
- 15 CCDC codes for supplementary crystallographic data for antiparallel-aligned (PhO, F)-azine: H. Bhoday, S. P. Kelley, A. Choudhury and R. Glaser, *CCDC Comm.*, 2020, 2013773 (XUXDIG, Ia, 100 K) and 2013774 (XUXDIG01, Ib, 293 K).
- 16 CCDC code for supplementary crystallographic data for parallel-aligned (PhO, F)-azine: H. Bhoday, S. P. Kelley and R. Glaser, *CCDC Comm.*, 2023, 2234129 (SIFGAT, IIa, 100 K).
- 17 E. Arunan and H. S. Gutowsky, *J. Chem. Phys.*, 1993, **98**, 4294–4296.
- 18 A. Katrusiak, M. Podsiadzo and A. Budzianowski, *Cryst. Growth Des.*, 2010, **10**, 3461–3465.
- 19 M. A. Spackman, A. S. Mitchell and J. J. McKinnon, *Chem. – Eur. J.*, 1998, **4**, 2136–2141.
- 20 M. A. Spackman and D. Jayatilaka, *CrystEngComm*, 2009, **11**, 19–32.
- 21 J. J. McKinnon, M. A. Spackman and A. S. Mitchell, *Acta Crystallogr., Sect. B: Struct. Sci.*, 2004, **60**, 627–668.
- 22 S. P. Thomas, P. R. Spackman, D. Jayatilaka and M. A. Spackman, *J. Chem. Theory Comput.*, 2018, **14**(3), 1614–1623.
- 23 C. F. Mackenzie, P. R. Spackman, D. Jayatilaka and M. A. Spackman, *IUcrJ*, 2007, 575–587.
- 24 A. Gavezzotti, *Acc. Chem. Res.*, 1994, **27**, 309–314.
- 25 B. P. van Eijck and J. Kroon, *J. Phys. Chem. B*, 1997, **101**, 1096–1100.
- 26 G. R. Desiraju and T. Steiner, *The Weak Hydrogen Bond in Structural Chemistry and Biology*, Oxford University Press, Oxford, UK, 1999.
- 27 V. R. Thalladi, H. C. Weiss, D. Blaser, R. Boese, A. Nangia and G. R. Desiraju, *J. Am. Chem. Soc.*, 1998, **120**, 8702–8710.
- 28 L. Shimoni and J. P. Glusker, *Struct. Chem.*, 1994, **5**, 383–397.
- 29 H. J. Schneider, *Chem. Sci.*, 2012, **3**, 1381–1394.
- 30 G. Kaur, P. Panini, D. Chopra and A. R. Choudhury, *Cryst. Growth Des.*, 2012, **12**, 5096–5110.